

Twelve nanometer half-pitch W–Cr–HSQ trilayer process for soft x-ray tungsten zone plates

Julia Reinspach,^{a)} Fredrik Uhlén, Hans M. Hertz, and Anders Holmberg
*Biomedical and X-Ray Physics, Department of Applied Physics, Royal Institute of Technology,
10691 Stockholm, Sweden*

received 23 June 2011; accepted 30 August 2011; published 29 September 2011)

The authors describe a new W–Cr–HSQ trilayer nanofabrication process for high-resolution and high-diffraction-efficiency soft x-ray W zone-plate lenses. High-resolution HSQ gratings were first fabricated by electron-beam lithography and high-contrast development in a NaCl/NaOH solution. The HSQ pattern was then transferred to the Cr layer by RIE with Cl₂/O₂, and subsequently to the W layer by cryogenic RIE with SF₆/O₂. The anisotropy of the W etch as a function of substrate temperature was investigated, and the best etch profile was achieved at –50 °C. Using this optimized process, W gratings with half-pitches down to 12 nm and a height of 90 nm were fabricated. For a zone plate with corresponding parameters, this would result in a theoretical diffraction efficiency of 9.6% (at $\lambda = 2.48$ nm), twice as high as has been reported previously. © 2011 American Vacuum Society. [DOI: 10.1116/1.3643760]

I. INTRODUCTION

In recent years soft x-ray microscopy has developed into a valuable research tool in numerous disciplines.¹ As the soft x-ray region contains various *K*- and *L*-absorption edges, it provides inherent element-specific contrast, thus allowing for element-sensitive imaging and chemical identification. For biological applications, the water window ($\lambda = 2.3$ – 4.4 nm) is of particular interest, since it provides natural contrast between water and proteins in combination with a high penetration depth (up to 10 μm), and therefore enables the imaging of whole hydrated cells in a near-native state without the need for staining or slicing. Due to the short wavelength of x rays, a very high resolution down to a few nanometers can theoretically be achieved. However, the imaging resolution is currently limited not by diffraction, but by the performance of the nanofabricated x-ray zone-plate lenses.

Zone-plate lenses are radially symmetric gratings with decreasing grating period from the center to the outermost part. The resolution of a zone-plate lens is directly proportional to the outermost zone width,² and therefore, to achieve high resolution, narrow zones have to be fabricated. In the past, zone widths down to 20 nm have been demonstrated by several research groups.^{3–5} To decrease the zone width further, sophisticated nanofabrication techniques have been employed. Recently, Chao *et al.*⁶ reported on Au zone plates with 12 nm outermost zone width fabricated by an advanced electron-beam overlay technique. Comamala *et al.*⁷ demonstrated 12.5 nm Ir zone plates for hard x-ray wavelengths using a frequency doubling process and atomic layer deposition. We have recently achieved 13 nm Ni and Ni–Ge zone plates by cold development of electron-beam-patterned ZEP7000 resist.^{8,9}

Apart from resolution, another important zone-plate property is its diffraction efficiency, which is defined as the fraction of incoming x-rays that is diffracted into the focus.

In imaging, a high efficiency is advantageous because it reduces the necessary exposure time to achieve a good signal-to-noise ratio in the x-ray images. Since the exposure time scales with the resolution to the power of -4 ,¹⁰ a good efficiency becomes especially important for high-resolution imaging. The diffraction efficiency is dependent on the zone height, the wavelength, and the zone material.¹¹ In Fig. 1, the theoretical efficiency is plotted for different soft x-ray optical materials as a function of zone height. It can be seen from the graph that optimum values are achieved for thicknesses of ~ 160 to ~ 370 nm, depending on the material. However, these heights cannot be reached, in practice, for narrow zones, due to the achievable aspect ratio in the nanofabrication. For example, the high-resolution Ni and Au zone plates presented earlier^{6,8} have zone heights of 35 nm or lower, resulting in a theoretical efficiency of less than 2%. Recently, we have also presented 13 nm Ni–Ge zone plates with a theoretical efficiency of 4.7%.⁹ It should be noted that in practice the efficiency of high-resolution zone plates is further reduced by about 50%,^{8,9} due to zone imperfections such as nonideal line-to-space ratio and line-edge roughness. Unfortunately, these imperfections cannot easily be avoided or corrected for at these small scales close to the resolution limit of the nanofabrication process. The low efficiency results in long exposure times in high-resolution x-ray imaging, typically in the range of a few tens of seconds for synchrotron-source microscopes, and substantially longer for present compact-source microscopes.^{6,12} This is a problem, as it makes the imaging more sensitive to drift, places high demands on the mechanical stability of the microscope, and possibly exposes the sample to a high radiation dose. All of these factors limit the potential applicability of sub-15 nm microscopy. Therefore, to promote the progress of high-resolution x-ray microscopy, it is necessary to improve not only the resolution, but also the diffraction efficiency of zone-plate lenses.

In the past, W has been used as optical material for zone plates in the hard x-ray region.¹³ However, as can be seen from Fig. 1, it is also an excellent material for soft x-ray

^{a)}Electronic mail: julia.reinspach@biox.kth.se

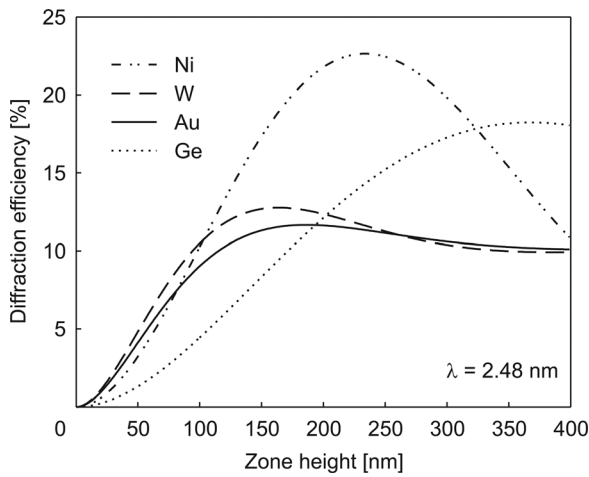


FIG. 1. Diffraction efficiency as a function of zone height for the materials Ni, Ge, Au, and W (at $\lambda = 2.48$ nm). For low zone heights, Au and W have the highest efficiencies.

zone plates, in particular for high-resolution zone plates with their relatively low zone heights. In addition, W can be structured by dry etching, thus allowing for an increased aspect-ratio and diffraction efficiency compared to electroplated Ni or Au zone plates.

In the present paper we describe a novel fabrication process for high-resolution soft x-ray W zone plates. The W is structured in a trilayer process, using Cr as hard mask and hydrogen silsesquioxane (HSQ) as electron-beam resist. Pattern transfer to the W layer is performed by RIE in an SF_6/O_2 plasma. The influence of substrate temperature on the W etch anisotropy is investigated, and high-resolution W gratings are presented.

II. FABRICATION PROCESS

Figure 2 illustrates the fabrication process for W structures. In summary, the grating pattern is first defined by electron-beam lithography [Fig. 2(b)], and subsequently transferred to the W layer by RIE [Figs. 2(c) and 2(d)].

First, a stack of materials was prepared on Si substrates. The stack consisted of a 10 nm Cr etch stop, 90 nm of W, a 6 nm Cr hard mask, and 10 nm of HSQ resist. The Cr hard mask served also as an HSQ sticking layer, since HSQ

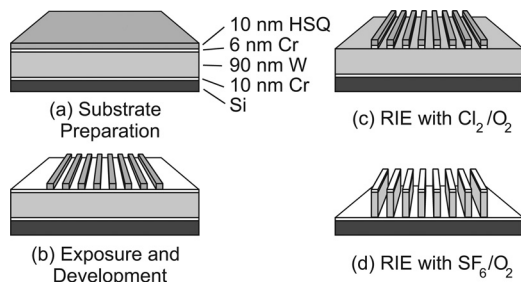


FIG. 2. Fabrication process for W gratings. After substrate preparation (a), the grating pattern is first written in the HSQ resist by electron-beam lithography and then developed (b). Subsequently, the pattern is transferred to the Cr layer by RIE with Cl_2/O_2 (c) and finally etched into the W by RIE with SF_6/O_2 (d).

exhibits poor adhesion to W. The Cr was deposited by electron-beam physical vapor deposition (Edwards Auto 306 system, 10^{-6} Torr base pressure) and the W layer was sputter deposited (AJA Orion system, 10^{-8} Torr base pressure). The HSQ layer was spincoated from a solution of 1% HSQ (XR-1541, Dow Corning) in methyl isobutyl ketone. No pre-exposure bake was performed. To avoid aging-related process instabilities,¹⁴ all samples were spin coated, electron-beam exposed, and developed within 1 day.

After substrate preparation, the HSQ was patterned by electron-beam lithography (Raith 150 system) at 25 kV and a dose of $\sim 2500 \mu\text{C}/\text{cm}^2$. The samples were then developed using a salty development process¹⁵ in an aqueous solution of 1 wt.% NaOH and 4 wt.% NaCl. After a development time of 60 s, the samples were first rinsed in H_2O for 5 min and then in isopropyl alcohol and in pentane for 15 s, respectively. The relative long rinse time in H_2O was necessary to dissolve all developer residues, which otherwise caused contamination problems in subsequent process steps.

The pattern was then transferred to the W layer by two steps of RIE. First, the pattern was etched into the Cr layer by RIE (Oxford Instruments, Plasmalab 100 system) with Cl_2/O_2 . The etching parameters were: 20 mTorr pressure, 8 sccm Cl_2 gas flow, 2 sccm O_2 gas flow, 40 W sample RF power, an etch time of 60 s, and a sample temperature of 20°C . The Cr then served as hard mask for the following W etch. This etch was performed by cryogenic RIE (Oxford Instruments, Plasmalab 100 system) with SF_6/O_2 at the following parameters: 10 mTorr pressure, 8 sccm SF_6 gas flow, 2 sccm O_2 gas flow, 40 W sample RF power, an etch time of 5 min, and a sample temperature of -50°C . At this temperature, a straight W etch profile was obtained. The effect of temperature on the W etch profile will be further discussed in Sec. III.

III. CRYOGENIC TUNGSTEN REACTIVE ION ETCHING

W etching in fluorine-based plasma is usually highly isotropic, and to achieve anisotropic etching, an inhibitor sidewall protection film is needed. Inhibitor films can be formed by low-temperature etching,^{16,17} and/or by the addition of an inhibitor film assisting gas (e.g., CHF_3 , H_2 , O_2 , N_2).^{16–19} In this section we present our results with low-temperature etching of high-resolution W structures in an SF_6/O_2 plasma.

Samples were prepared as described in Sec. II. To ensure comparability, all samples were prepared on one wafer and cut up in individual pieces before the RIE etch steps. After the Cr RIE, the samples were etched in SF_6/O_2 at different temperatures. Figure 3 shows cross sections of tungsten gratings with 14 nm half-pitch, etched at -100 , -50 , -40 , and -20°C . At -20°C , the etching is isotropic, resulting in mask undercut and linewidth loss, and finally pattern collapse. Reducing the temperature results in an increased sidewall passivation effect. At -100°C , sidewall passivation is too high, leading to a sloped line profile and preventing clearing of the structures. The most vertical sidewalls were

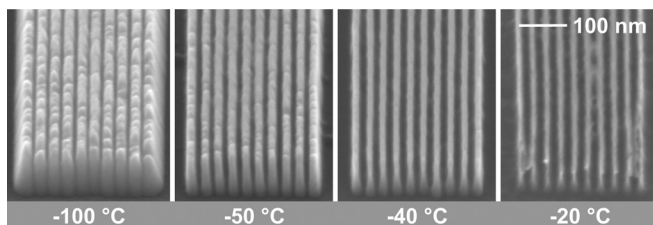


FIG. 3. Tungsten gratings with 14 nm half-pitch etched at different temperatures. Best results are achieved at a substrate temperature of $-50\text{ }^{\circ}\text{C}$. For $-20\text{ }^{\circ}\text{C}$, the etching is isotropic, resulting in undercut of the Cr mask and linewidth loss. For $-100\text{ }^{\circ}\text{C}$, sidewall passivation is too high, yielding sloped sidewalls.

obtained at a temperature of $-50\text{ }^{\circ}\text{C}$, which was therefore considered to be the optimum etch temperature.

It should be noted, however, that these parameters seem to be specific for this W–Cr–HSQ trilayer system, and that it may be necessary to adjust them for other processes. For example, for gratings with a half-pitch of 50 nm and larger, which were fabricated with the same experimental equipment, but by a W–Cr–ZEP7000 trilayer process, a temperature of $-20\text{ }^{\circ}\text{C}$ yielded best results.²⁰ The reason for this may be an increased sidewall passivation effect due to the use of ZEP7000 instead of HSQ. Etched and sputtered ZEP7000 may redeposit on the grating sidewalls, which would enhance the film forming effect and therefore allow etching at higher temperatures.

IV. RESULTS: TUNGSTEN GRATINGS

The above-described optimized process was used to fabricate W gratings. Figure 4 shows gratings with half-pitches from 14 down to 11 nm and a W height of 90 nm. The quality of the lines is good, with a straight line profile and a line-to-space ratio of close to 1:1. From the SEM images it can be seen that the Cr mask has eroded away for the 11 nm half-pitch lines, resulting in etching of the underlying W and therefore a slightly reduced W height. For the 12 nm lines, the mask is partly gone, but the height of the structures is not

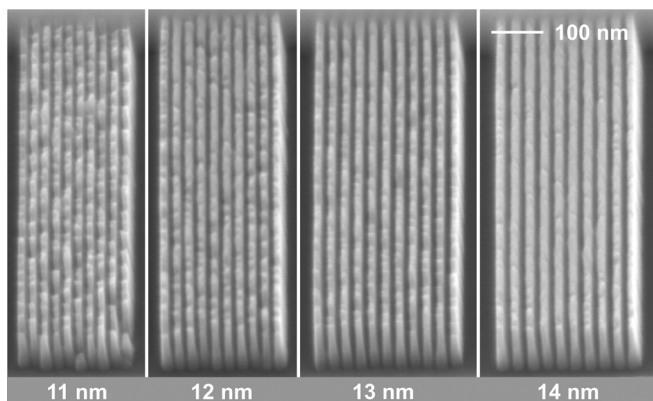


FIG. 4. W gratings with half-pitches of 11–14 nm. The W height is 90 nm. The pattern transfer for lines with half-pitches down to 12 nm is good. For the 11 nm lines, the Cr mask has eroded and the underlying W is partly etched away.

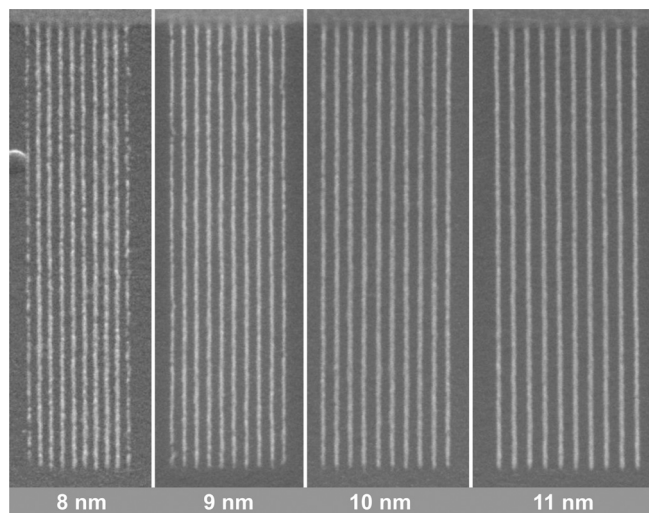


FIG. 5. HSQ gratings on an Si substrate without a W layer with half-pitches of 8–11 nm. The HSQ height is 10 nm. On only a Si substrate, a higher resolution can be obtained than for exposures on a W substrate.

severely decreased. Currently, this mask erosion seems to be the limiting factor for the achievable aspect ratio in the W etch. A thicker Cr mask was tested, but the pattern transfer from HSQ to the Cr layer did not yield good results at this high resolution.

For the W process described here, the best resolution which was obtained was 11 nm half-pitch lines. Smaller lines were not resolved in the resist, but resist residues remained in between the exposed lines. We are convinced that the comparatively low resolution on W substrates is a result of backscattered electrons, due to the high atomic number of W. In fact, a clearly higher resolution was obtained when fabricating HSQ gratings directly on an Si substrate. This is illustrated in Fig. 5, where nicely resolved gratings with half-pitches down to 8 nm are shown.

V. SUMMARY AND OUTLOOK

In this paper we presented a new W–Cr–HSQ trilayer process for the fabrication of high-resolution high-diffraction-efficiency soft x-ray W zone plates. Salty development of HSQ was applied and 11-nm half-pitch resolution in the resist was achieved on high-Z W substrates. On Si substrates with no W layer, a resolution of 8 nm half-pitch in HSQ was reached. Cryogenic RIE of W in an SF_6/O_2 plasma was investigated to find optimum process conditions for high anisotropy. With an optimized process, W gratings with half-pitches of 12 nm and a tungsten height of 90 nm were fabricated.

This process will be used to fabricate high-resolution soft x-ray zone plates. A zone plate with a W height of 90 nm would have a theoretical diffraction efficiency of 9.6% (at $\lambda = 2.48\text{ nm}$), and an expected actual efficiency of about half that value. This would be twice the efficiency that can currently be reached with state-of-the-art 13 nm Ni–Ge zone plates,⁹ and four times higher than for state-of-the-art 13 nm Ni zone plates.⁸

ACKNOWLEDGMENTS

The authors gratefully acknowledge the financial support of the Swedish Science Research Council, the Swedish Foundation for Strategic Research, and the Wallenberg Foundation.

- ¹*Proceedings of the Ninth International Conference on X-Ray Microscopy*, edited by C. David, F. Nolting, F. Pfeiffer, C. Quitmann, and M. Stampantoni [J. Phys. Conf. Ser. **186** (2009)].
- ²D. T. Attwood, *Soft X-Rays and Extreme Ultraviolet Radiation* (Cambridge University Press, Cambridge, 1999), pp. 337–394.
- ³M. Peuker, *Appl. Phys. Lett.* **78**, 2208 (2001).
- ⁴Y. Feng, M. Feser, A. Lyon, S. Rishton, X. Zeng, S. Chen, S. Sassolini, and W. Yun, *J. Vac. Sci. Technol. B* **25**, 2004 (2007).
- ⁵M. Lindblom, J. Reinspach, O. von Hofsten, M. Bertilson, H. M. Hertz, and A. Holmberg, *J. Vac. Sci. Technol. B* **27**, L1 (2009).
- ⁶W. Chao, J. Kim, S. Rekawa, P. Fischer, and E. H. Anderson, *Opt. Express* **17**, 17669 (2009).
- ⁷J. Vila-Comamala, K. Jefimovs, J. Raabe, T. Pilvi, R. H. Fink, M. Senoner, A. Maaßdorf, M. Ritala, and C. David, *Ultramicroscopy* **109**, 1360 (2009).
- ⁸J. Reinspach, M. Lindblom, O. von Hofsten, M. Bertilson, H. M. Hertz, and A. Holmberg, *J. Vac. Sci. Technol. B* **27**, 2593 (2009).
- ⁹J. Reinspach, M. Lindblom, O. von Hofsten, M. Bertilson, H. M. Hertz, and A. Holmberg, *J. Vac. Sci. Technol. B* **29**, 011012 (2011).
- ¹⁰D. Sayre, J. Kirz, R. Federer, D. M. Kim, and E. Spiller, *Ultramicroscopy* **2**, 337 (1977).
- ¹¹J. Kirz, *J. Opt. Soc. Am.* **64**, 301 (1974).
- ¹²O. von Hofsten, M. Bertilson, J. Reinspach, A. Holmberg, H. M. Hertz, and U. Vogt, *Opt. Lett.* **34**, 2631 (2009).
- ¹³P. Charalambous, *AIP Conf. Proc.* **507**, 625 (2000).
- ¹⁴F. C. M. J. M. van Delft, *J. Vac. Sci. Technol. B* **20**, 2932 (2002).
- ¹⁵J. K. W. Yang and K. K. Berggren, *J. Vac. Sci. Technol. B* **25**, 2025 (2007).
- ¹⁶A. L. Goodyear, S. Mackenzie, D. L. Olynick, and E. H. Anderson, *J. Vac. Sci. Technol. B* **18**, 3471 (2000).
- ¹⁷C. W. Jurgensen, R. R. Kola, A. E. Novembre, W. W. Tai, J. Frackowiak, L. E. Trimble, and G. K. Celler, *J. Vac. Sci. Technol. B* **9**, 3280 (1991).
- ¹⁸W. Chu *et al.*, *Appl. Phys. Lett.* **64**, 2172 (1994).
- ¹⁹D. M. Tennant, S. C. Shunk, M. D. Feuer, J.-M. Kuo, R. E. Behringer, T. Y. Chang, and R. W. Epworth, *J. Vac. Sci. Technol. B* **7**, 1836 (1989).
- ²⁰F. Uhlén, S. Lindqvist, D. Nilsson, J. Reinspach, R. Barrett, U. Vogt, H. M. Hertz, and A. Holmberg, *J. Vac. Sci. Technol. B* (2011) (to be published).